Journal of Power Sources 246 (2014) 19–23

Contents lists available at SciVerse ScienceDirect

Journal of Power Sources

journal homepage: www.elsevier.com/locate/jpowsour

Short communication

Spinel $LiMn_2O_4$ nanohybrid as high capacitance positive electrode material for supercapacitors

F.X. Wang [a], S.Y. Xiao [a], Y.S. Zhu [a], Z. Chang [a], C.L. Hu [a], Y.P. Wu [a,*], R. Holze [b]

[a] New Energy and Materials Laboratory (NEML), Department of Chemistry & Shanghai Key Laboratory of Molecular Catalysis and Innovative Materials, Fudan University, Shanghai 200433, China
[b] Technische Universität Chemnitz, Institut für Chemie, AG Elektrochemie, D-09107 Chemnitz, Germany

HIGHLIGHTS

- $LiMn_2O_4$ nanohybrid has been prepared using α-MnO_2 nanotubes and LiOH at 700 °C.
- It consists of nanotubes, nanorods and nanoparticles.
- Its formation mechanism is explained.
- It exhibits a high specific capacitance of 415 F g^{-1} at 0.5 A g^{-1} in 0.5 mol l^{-1} Li_2SO_4 aqueous solution.
- A supercapacitor using $LiMn_2O_4$ nanohybrid as the positive electrode in aqueous solution presents good cycling.

ARTICLE INFO

Article history:
Received 14 May 2013
Received in revised form
5 July 2013
Accepted 8 July 2013
Available online 16 July 2013

Keywords:
Supercapacitors
Lithium manganese oxide
Nanohybrid
Aqueous electrolyte
Manganese oxide nanotube

ABSTRACT

A $LiMn_2O_4$ nanohybrid consisting of nanotubes, nanorods and nanoparticles has been synthesized using α-MnO_2 nanotubes from hydrothermal reaction as a precursor. It is characterized with X-ray diffraction, field emission scanning electron and transmission electron microscopy. A formation mechanism is proposed. As a positive electrode material for supercapacitors, it exhibits a high specific discharge capacitance of 415 F g^{-1} at 0.5 A g^{-1} in 0.5 mol l^{-1} Li_2SO_4 aqueous solution. Even at 10 A g^{-1}, it still has a specific discharge capacitance of 208 F g^{-1}. The energy density of the asymmetric supercapacitor using activated carbon as the negative electrode and $LiMn_2O_4$-nanohybrid as the positive electrode in the aqueous solution in the voltage range of 0–1.8 V presents 29.8 Wh kg^{-1} at power density of 90 W kg^{-1}. In addition, the cycling behavior of the asymmetric supercapacitor is good.

1. Introduction

Systems for electrochemical energy storage and conversion including batteries, fuel cells, and supercapacitors have attracted considerable attention in recent years since they can increase the energy efficiency, reduce emission of greenhouse gases and promote the use of renewable energy [1]. Supercapacitors can be coupled with batteries and fuel cells to provide peak power in the next generation all-electric cars and replace batteries for memory back-up, which makes them probably one of the most important next-generation energy storage devices [1–3]. Materials like carbon nanotubes (CNTs), activated carbon, conducting polymers and metal oxides including MoO_3, RuO_2, MnO_2 and V_2O_5 have been explored as electrode materials for supercapacitors to increase the energy density [4–11].

Nanostructured materials as electrode materials for electrochemical energy storage systems have shown some advantages such as higher capacitance and better rate capability over traditional micrometer-sized materials [12–16]. Among them one-dimensional (1D) nanostructures including nanowires, nanotubes and nanorods have attracted special attention. For example, nanostructured $LiMn_2O_4$ in the form of nanorods, nanowires, nanopores and nanotubes has been well investigated as electrode materials in aqueous electrolytes [13–16]. According to our knowledge, there have been no reports on nanohybrids which consist of several nano-structures of the same material as electrode materials for supercapacitors.

* Corresponding author.
E-mail addresses: wuyp@fudan.edu.cn (Y.P. Wu), rudolf.holze@chemie.tu-chemnitz.de (R. Holze).

0378-7753/$ – see front matter © 2013 Elsevier B.V. All rights reserved.
http://dx.doi.org/10.1016/j.jpowsour.2013.07.046

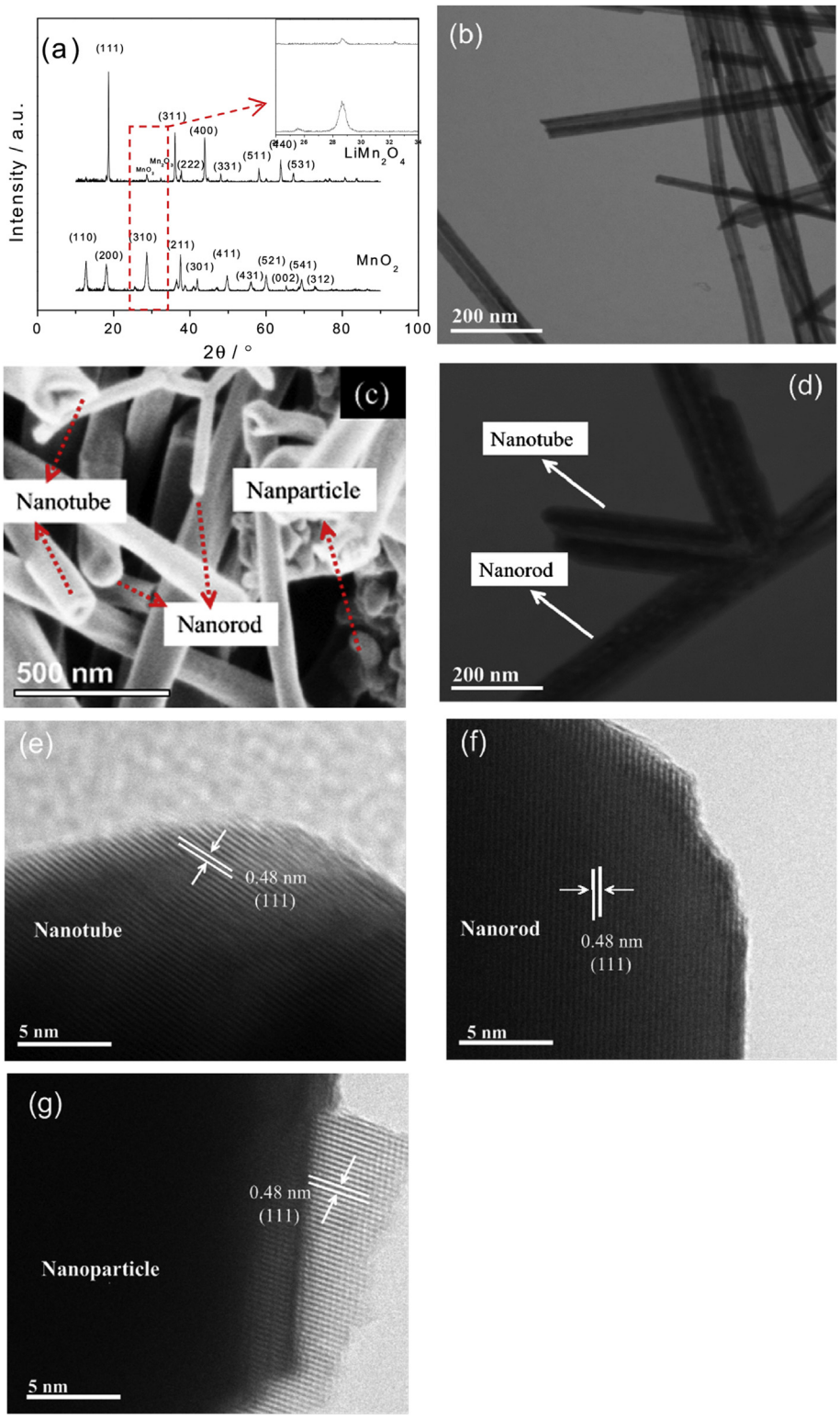

Fig. 1. Some physical properties of the prepared α-MnO_2 nanotubes and LMO-NH: (a) XRD patterns of α-MnO_2 nanotubes and LMO-NH, (b) TEM micrograph of α-MnO_2 nanotubes, (c) FESEM, (d) TEM, (e) (f) and (g) HRTEM micrographs of LMO-NH.

In this paper, we report on a $LiMn_2O_4$ nanohybrid (LMO-NH) consisting of nanotubes, nanorods and nanoparticles. Interestingly, this nanohybrid shows excellent electrochemical performance in 0.5 mol l^{-1} Li_2SO_4 aqueous solution as positive electrode material for supercapacitors.

2. Experimental

Alpha-MnO_2 nanotubes were prepared by a hydrothermal method [17] with minor modifications. $MnCl_2 \cdot 4H_2O$ (0.3562 g) was dissolved in 40 ml distilled water, 0.0445 g NH_4F was added as

template, then $KMnO_4$ (0.1896 g) was added to this solution under constant stirring. Finally, the mixed solution was transferred into a Teflon-lined stainless steel autoclave with a volume of 50 ml, and maintained at 180 °C for 24 h. After the reaction was finished, the resulting solid product was filtered off, washed with distilled water and ethanol, and dried at 80 °C in air. The as-prepared MnO_2 was added into LiOH solution (molar ratio of Li/Mn = 1:2) at 25 °C, then sonicated about 0.5 h and dried at 80 °C in air under vigorous stirring. After the water was evaporated, the mixture was transferred into a furnace and heat-treated at 700 °C for 10 h to get LMO-NH. The rising rate of temperature was 3 °C min^{-1}. All chemicals were of analytical grade, and the aqueous solutions were prepared with distilled water.

The positive electrodes were prepared by mixing thoroughly the prepared LMO-NH, acetylene black and polytetrafluoroethylene in a weight ratio of 8:1:1. The mixture was pressed into a film and dried at 120 °C overnight. After drying, the film was cut into disks of about 1.5 mg (0.25 cm^2). These disks were pressed onto a Ni-grid at a pressure of 20 MPa to act as working electrodes. Activated carbon (AC) electrodes were prepared in the same way as the LMO-NH electrodes [15,16]. The AC was purchased from Ningde Xinseng Chemical Industrial Co., Ltd. and has a specific surface area of about 2800 m^2 g^{-1} measured by the Brunnauer–Emmet–Teller (BET) method.

The X-ray diffraction (XRD) patterns were collected using a Rigaku D/MAX-IIA X-ray diffractometer with Cu K_α radiation. Field emission scanning electron micrographs (FESEM) were obtained with a FE-SEM-4800-1, transmission electron micrographs (TEM) with a JEM-2100F (JEOL). Cyclic voltammograms (CV) and galvanostatic charge and discharge tests were performed in 0.5 mol l^{-1} Li_2SO_4 aqueous solution with a three-electrode cell, where the AC electrode and a saturated calomel electrode (SCE) were used as the counter and the reference electrodes, respectively, by an electrochemical station (Chenhua, China). A two-electrode cell consisting of the above LMO-NH working electrode and the AC counter electrode with a distance of about 1 cm was used to test the cycling behavior between 0 and 1.8 V by a Land tester. All electrochemical tests were carried out at room temperature.

The specific discharge capacity C (F g^{-1}) is calculated according to the following Equation (1) [18,19]:

$$C = (I\Delta t)/(m\Delta V) \quad (1)$$

where I (mA) is the applied working current, Δt (s) represents the discharge time, ΔV (V) is the voltage range, and m (g) is the mass of active materials. All electrochemical data were calculated based on the mass of the active spinel LMO-NH material.

3. Results and discussion

The X-ray diffraction (XRD) patterns of the samples shown in Fig. 1a indicates that the prepared MnO_2 nanotubes and LMO-NH can be indexed as the pure tetragonal α-MnO_2 phase (JCPDS 44-0141) and the spinel $LiMn_2O_4$ phase, respectively [13,15]. Of course, there are minor amounts of impure phases, which are ascribed to Mn_2O_3 and unreacted MnO_2. The main reason is that the heat-treatment process made some lithium evaporated, and therefore there was not enough lithium to react with the Mn oxides. The TEM micrograph (Fig. 1b) shows well-shaped nanotubes of MnO_2. In the case of the LMO-NH (Fig. 1c and d), not only nanotubes but also nanorods and nanoparticles can be observed. The HRTEM micrographs (Fig. 1e, f and g) shows the atom arrangements of nanotubes, nanorods and nanoparticles, and the measured spacing of 0.48 nm can be indexed to the distance between (111) planes of $LiMn_2O_4$ [14]. The formation process of the spinel LMO-NH can be schematically illustrated in Scheme 1. At first, the α-MnO_2 spontaneously grows and tubular samples are obtained in the presence of F^--anions, which act as a template for nanotubes [20,21]. During the following calcination process, some MnO_2 nanotubes can still retain the tubular morphology to form $LiMn_2O_4$ nanotubes and part of MnO_2 nanotubes will be split into shorter nanotubes of different length due to the high temperature and the reaction with LiOH. With the increase of calcination time, these incomplete short nanotubes will be transformed into $LiMn_2O_4$ nanorods, and those with very short length will produce $LiMn_2O_4$ nanoparticles.

The CV curves of the LMO-NH at different scan rates are presented in Fig. 2a. The shapes of the CV curves indicate that the capacitive behavior of the LMO-NH is different from that of a plain electric double-layer capacitance (such as AC), which produces a rectangle-like curve. The CVs of the LMO-NH at different scan rates present two couples of redox peaks which are consistent with the deintercalation and intercalation of Li^+ ions from/into the host spinel structure [13–16].

The charge–discharge profiles of the LMO-NH electrodes at different current densities in the first cycle are shown in Fig. 2b. The LMO-NH exhibits a specific discharge capacitance of 415 F g^{-1} at 0.5 A g^{-1}. The two plateaus during charge/discharge are observed in agreement with the CV curves and previous reports [13–16]. The capacitance is higher than those reported for $LiMn_2O_4$ and most MnO_2-materials [8,22,23]. At a high specific current of 5 A g^{-1}, it can still deliver a specific discharge capacitance of 359 F g^{-1}, nearly 87% of its capacitance at 0.5 A g^{-1}. Meanwhile, a specific discharge capacitance of 208 and 175 F g^{-1} can be achieved when the specific current is increased to 10 and 12 A g^{-1}, respectively. So far, according to our knowledge hardly such high specific discharge capacitance at such large charge current density for $LiMn_2O_4$ as positive electrodes has been reported. When the LMO-NH electrode is first charged at the low specific current of 0.4 A g^{-1} and then discharged at different specific currents, the obtained discharge curves are shown in Fig. 2c. The LMO-NH electrode can deliver 390 and 310 F g^{-1} at 2.7 and 6.6 A g^{-1}, respectively, indicating that the rate behavior of the LMO-NH in aqueous electrolyte is also much better than that of the most recently reported V_2O_5/CNT composites [24] and MnO_2-nanosphere/

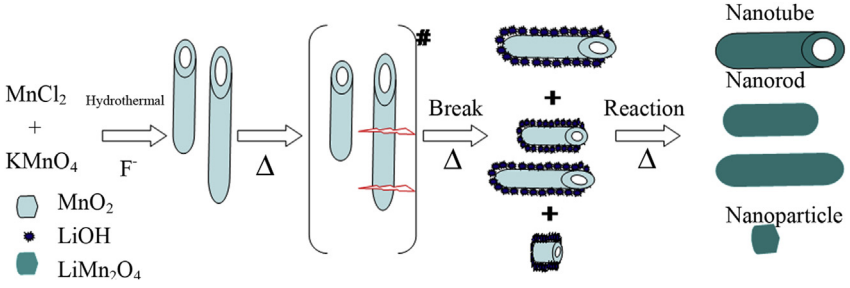

Scheme 1. The formation process of $LiMn_2O_4$ nanohybrid (LMO-NH).

carbon nanotubes/conducting polymer ternary composites [12]. Evidently, the superior electrochemical performance is due to the unique nanohybrid structure of our as-prepared $LiMn_2O_4$. Whether nanotubes, nanorods or nanoparticles, they all have high electrode/electrolyte contact area and short lithium diffusion distance, which will reduce the lithium diffusion distance during the Faradaic redox reactions, so this nanohybrid can be a good positive electrode material for supercapacitors.

Fig. 3a shows the charge and discharge curves of the AC electrode, of the LMO-NH electrode and of the asymmetric supercapacitor consisting of AC and LMO-NH electrodes using 0.5 mol l^{-1} Li_2SO_4 aqueous solution as the electrolyte at 3 A g^{-1} based on the LMO-NH material. In case of the asymmetric supercapacitor, the weight ratio of AC to LMO-NH is 2.9:1. The asymmetric

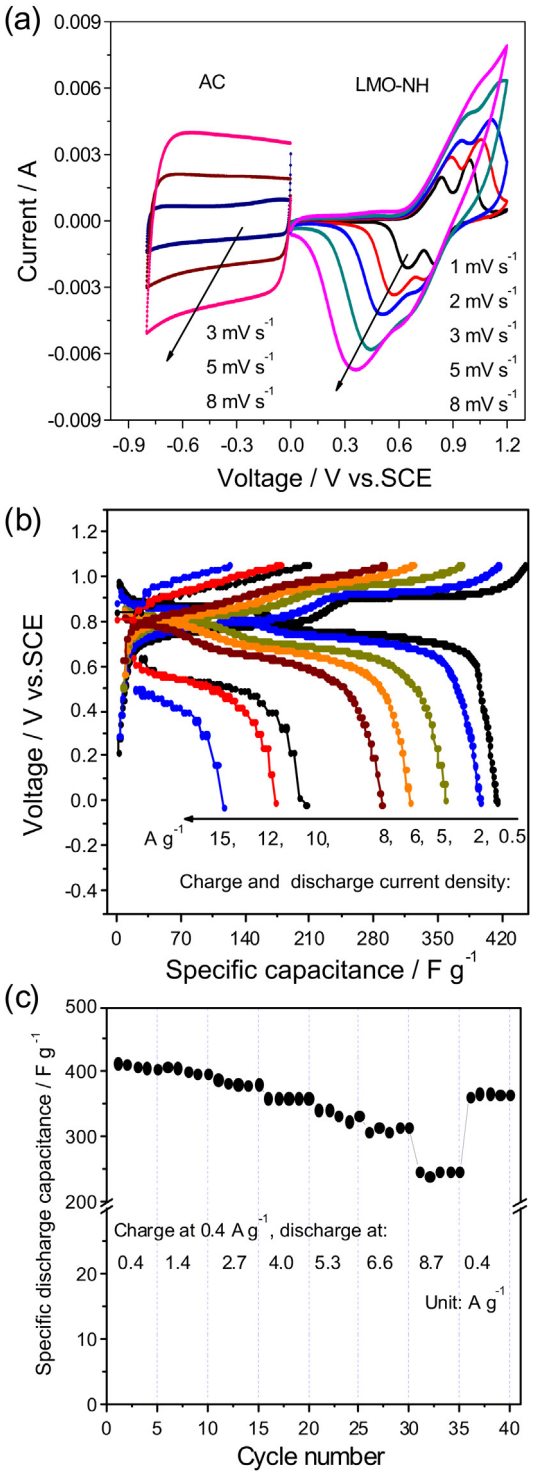

Fig. 2. Electrochemical performance of the prepared LMO-NH: (a) cyclic voltammogram, (b) the first galvanostatic charge and discharge curves at various mass activity, (c) the specific discharge capacitance at different current densities when charged at 0.4 A g^{-1}. The other electrochemical data were calculated based on the mass of the LMO-NH.

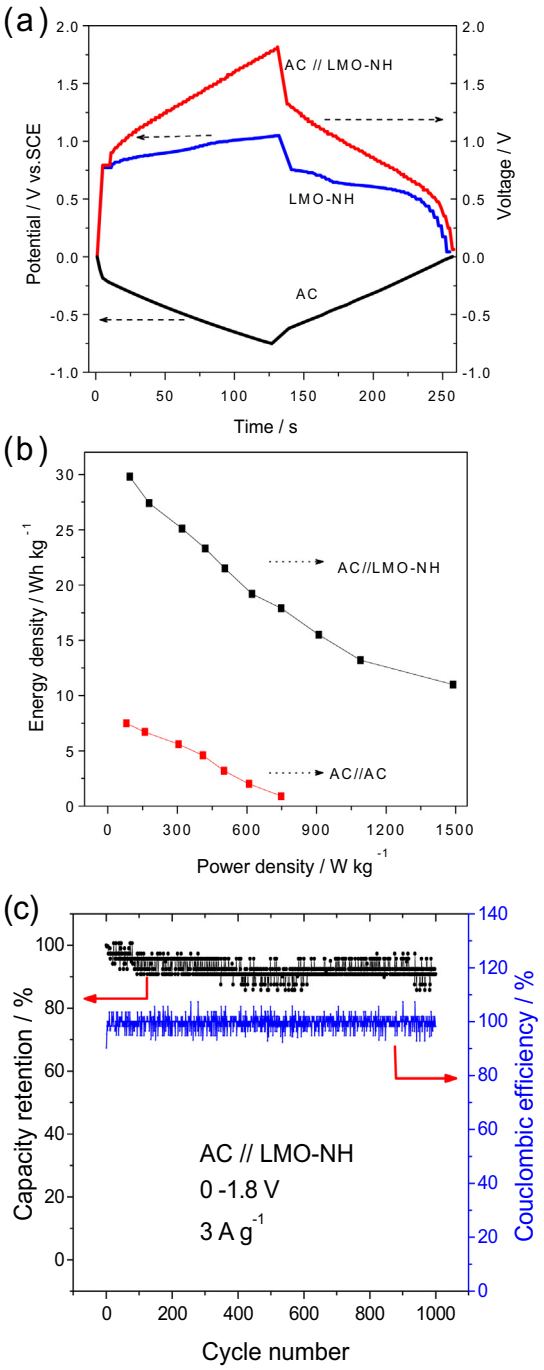

Fig. 3. (a) The potential–time curves of the individual electrodes vs. SCE reference electrode and the voltage–time profile of the asymmetric AC//LMO-NH supercapacitor at 3 A g^{-1}, (b) Ragone plots of the supercapacitor AC//LMO-NH and AC//AC, and (c) the cycling behavior and Coulombic efficiency of AC//LMO-NH at 3 A g^{-1}. The Ragone plot was calculated based on the total mass of LMO-NH and AC, and the other electrochemical data were calculated based on the mass of the LMO-NH.

supercapacitor shows a sloping voltage–time profile from 0 to 1.8 V. The Ragone plots of the asymmetric supercapacitor based on AC/0.5 mol l^{-1} Li_2SO_4/LMO-NH and the symmetric supercapacitor based on AC/0.5 mol l^{-1} Li_2SO_4/AC are shown in Fig. 3b. The asymmetric supercapacitor presents an energy density of 29.8 Wh kg^{-1} at power density of 90 W kg^{-1}, much higher than that of the symmetric AC//AC capacitor. Moreover, it keeps an energy density of 11.2 Wh kg^{-1} at power density of 1500 W kg^{-1}. The cycling behavior of this supercapacitor in the voltage range of 0–1.8 V at 3 A g^{-1} is shown in Fig. 3c, which is also superior to the reported $LiMn_2O_4$ in the aqueous electrolytes [14,22,23]. The capacity retention is 91% after 1000 cycles. Moreover, the Coulombic efficiency is almost 100% after the initial cycle. To the best of our knowledge, this is the first time to synthesize $LiMn_2O_4$ nanohybrid as a positive electrode material for asymmetric supercapacitor in aqueous electrolyte. Recently, nanostructured spinel $LiMn_2O_4$ materials with various morphologies including nanoparticles [25–27], nanorods [17,28–32], nanowires [33–35] and nanotubes [16,36–39] have been extensively investigated to improve rate capabilities for lithium ion batteries in organic and aqueous electrolytes. For example, the electrochemical performance can be improved by using $LiMn_2O_4$ nanorods [17,28–32]. It was found that such morphology improved the kinetics at very high current density and was capable of the facile structural transformation between the cubic phase and the tetragonal one [29]. A comparison of the morphology difference between the bulk and the nanorod $LiMn_2O_4$ recovered from hydrostatic pressure conditions also indicates that the nanorod $LiMn_2O_4$ could accommodate more stress and strain compared to its bulk counterpart [40]. The tubular spinel $LiMn_2O_4$ could preserve preferential growth direction and microstructural stability essentially, even after long-term cycling at relatively high rates [38]. The solid nanoparticles are expected to guarantee high volumetric and weight energy density because the hollow $LiMn_2O_4$ nanotubes have low tap density [41]. Therefore, the $LiMn_2O_4$ nanohybrid, in our case, also presents superior high-power performance in the aqueous electrolyte because it combines the advantages of nanoparticles, nanorods and nanotubes.

4. Conclusions

A $LiMn_2O_4$ nanohybrid consisting of nanotubes, nanorods and nanoparticles was prepared successfully by the reaction of hydrothermally prepared α-MnO_2 nanotubes with LiOH at 700 °C. Under the action of high temperature and LiOH, some MnO_2 nanotubes retain the shape and produce $LiMn_2O_4$ nanotubes, however, some were split into nanotube fragments with different lengths. As a result, those incomplete nanotubes form $LiMn_2O_4$-nanorods and the very short ones transform into $LiMn_2O_4$ nanoparticles with the increase of calcination time. The nanohybrid shows high specific discharge capacitance in 0.5 mol l^{-1} Li_2SO_4 aqueous solution, which can be 415 F g^{-1} and 208 F g^{-1}, respectively, at the specific currents of 0.5 A g^{-1} up and 10 A g^{-1}. Its cycling performance at 3 A g^{-1} when tested as supercapacitors using activated carbon as the negative electrode in the aqueous solution is good, and the capacitance retention is 91% after 1000 cycles.

Acknowledgments

Financial support from MOST Programs (2010DFA61770), NSFC (21073046) and Partnership of Alexander von Humboldt Foundation is gratefully appreciated.

References

[1] X. Wang, Y. Hou, Y. Zhu, Y. Wu, R. Holze, Sci. Rep. 3 (2013) 1401.
[2] X. Du, C. Wang, M. Chen, Y. Jiao, J. Wang, J. Phys. Chem. C 113 (2009) 2643.
[3] W. Tang, L.L. Liu, S. Tian, L. Li, Y.B. Yue, Y.P. Wu, K. Zhu, Chem. Commun. 47 (2011) 10058.
[4] S.W. Lee, N. Yabuuchi, B.M. Gallant, S. Chen, B.S. Kim, P.T. Hammond, Y.S. Horn, Nat. Nanotechnol. 5 (2010) 531.
[5] Y.P. Wu, E. Rahm, R. Holze, J. Power Sources 114 (2003) 228.
[6] H.L. Wang, Q.L. Hao, X.J. Yang, L.D. Lu, X. Wang, Electrochem. Commun. 11 (2009) 1158.
[7] C.C. Hu, C.C. Wang, Electrochem. Commun. 4 (2002) 554.
[8] R. Liu, S.B. Lee, J. Am. Chem. Soc. 130 (2008) 2942.
[9] M. Sathiya, A.S. Prakash, K. Ramesha, J.M. Tarascon, A.K. Shukla, J. Am. Chem. Soc. 113 (2011) 16291.
[10] Y. Guo, J. Hu, L. Wan, Adv. Mater. 20 (2008) 2878.
[11] F. Wang, S. Xiao, Y. Hou, C. Hu, L. Liu, Y. Wu, RSC Adv. 3 (2013), http://dx.doi.org/10.1039/C3RA23466E.
[12] Y. Hou, Y. Cheng, T. Hobson, J. Liu, Nano Lett. 10 (2010) 2727.
[13] W. Tang, S. Tian, L.L. Liu, L. Li, H.P. Zhang, Y.B. Yue, Y. Bai, Y.P. Wu, K. Zhu, Electrochem. Commun. 13 (2011) 205.
[14] M. Zhao, X. Song, F. Wang, W. Dai, X. Lu, Electrochim. Acta 56 (2011) 5673.
[15] Q.T. Qu, L.J. Fu, X.Y. Zhan, D. Samuelis, J. Maier, L. Li, S. Tian, Z.H. Li, Y.P. Wu, Energy Environ. Sci. 4 (2011) 3985.
[16] W. Tang, Y. Hou, F. Wang, L. Liu, Y. Wu, K. Zhu, Nano Lett. 13 (2013) 2036.
[17] D.K. Kim, P. Muralidharan, H.W. Lee, R. Ruffo, Y. Yang, C.K. Chan, H.L. Peng, R.A. Huggins, Y. Cui, Nano Lett. 8 (2008) 3948.
[18] X. Xia, J. Tu, Y. Mai, X. Wang, C. Gu, X. Zhao, J. Mater. Chem. 21 (2011) 9319.
[19] J. Feng, X. Sun, C. Wu, L. Peng, C. Lin, S. Hu, J. Yang, Y. Xie, J. Am. Chem. Soc. 133 (2011) 17832.
[20] N.K. Allam, M.A. ElSayed, J. Phys. Chem. C 114 (2010) 12024.
[21] W. Wei, K. Lee, S. Shaw, P. Schmuki, Chem. Commun. 48 (2012) 4244.
[22] I.B. Stojkovic, N.D. Cvjeticanin, S.V. Mentus, Electrochem. Commun. 12 (2010) 371.
[23] F.X. Wang, S.Y. Xiao, Y. Shi, L.L. Liu, Y.S. Zhu, Y.P. Wu, J.Z. Wang, R. Holze, Electrochim. Acta 93 (2013) 301.
[24] Z. Chen, Y. Qin, D. Weng, Q. Xiao, Y. Peng, X. Wang, H. Li, F. Wei, Y. Lu, Adv. Funct. Mater. 19 (2009) 3420.
[25] K.M. Shaju, P.G. Bruce, Chem. Mater. 20 (2008) 5557.
[26] S. Lee, Y. Cho, H.K. Song, K.T. Lee, J. Cho, Angew. Chem. Int. Ed. 51 (2012) 8748.
[27] L. Xiao, Y. Guo, D. Qu, B. Deng, H. Liu, D. Tang, J. Power Sources 225 (2013) 286.
[28] Y. Yang, C. Xie, R. Ruffo, H. Peng, D.K. Kim, Y. Cui, Nano Lett. 9 (2009) 4109.
[29] F. Cheng, H. Wang, Z. Zhu, Y. Wang, T. Zhang, Z. Tao, J. Chen, Energy Environ. Sci. 4 (2011) 3668.
[30] Z. Bai, N. Fan, Z. Ju, C. Sun, Y. Qian, Mater. Lett. 76 (2012) 124.
[31] L. He, S. Zhang, X. Wei, Z. Du, G. Liu, Y. Xing, J. Power Sources 220 (2012) 228.
[32] X. Xiang, Z. Fu, W. Li, J. Solid State Electrochem. 17 (2013) 1201.
[33] E. Hosono, T. Kudo, I. Honma, H. Matsuda, H.S. Zhou, Nano Lett. 9 (2009) 1045.
[34] H.W. Lee, P. Muralidharan, R. Ruffo, C.M. Mari, Y. Cui, D.K. Kim, Nano Lett. 10 (2010) 3852.
[35] S. Lee, Y. Oshima, E. Hosono, H.S. Zhou, K. Takayanagi, Ultramicroscopy 125 (2013) 43.
[36] N. Li, C.J. Patrissi, G. Che, C.R. Martin, J. Electrochem. Soc. 147 (2000) 2044.
[37] X. Li, F. Cheng, B. Guo, J. Chen, J. Phys. Chem. B 109 (2005) 14017.
[38] Y.L. Ding, J. Xie, G.S. Cao, T.J. Zhu, H.M. Yu, X.B. Zhao, Adv. Funct. Mater. 21 (2011) 348.
[39] Y.L. Ding, J. Xie, G.S. Cao, T.J. Zhu, H.M. Yu, X.B. Zhao, J. Phys. Chem. C 115 (2011) 9821.
[40] Y. Lin, Y. Yang, H. Ma, Y. Cui, W.L. Mao, J. Phys. Chem. C 115 (2011) 9844.
[41] Y. Wu, Z. Wen, H. Feng, J. Li, Small 8 (2012) 858.